HHS Public Access

Author manuscript

Cell Rep. Author manuscript; available in PMC 2024 May 20.

Published in final edited form as:

Cell Rep. 2024 April 23; 43(4): 114120. doi:10.1016/j.celrep.2024.114120.

CCR2+ monocytes replenish border-associated macrophages in the diseased mouse brain

Lingxiao Wang[1,2], **Jiaying Zheng**[1,2], **Shunyi Zhao**[1,2], **Yushan Wan**[1], **Meijie Wang**[3], **Dale B. Bosco**[1], **Chia-Yi Kuan**[4], **Jason R. Richardson**[5], **Long-Jun Wu**[1,6,7,8,*]

[1]Department of Neurology, Mayo Clinic, Rochester, MN 55905, USA

[2]Mayo Clinic Graduate School of Biomedical Sciences, Rochester, MN 55905, USA

[3]Department of Molecular Pharmacology and Experimental Therapeutics, Mayo Clinic, Rochester, MN 55905, USA

[4]Department of Neuroscience, University of Virginia School of Medicine, Charlottesville, VA 22908, USA

[5]Department of Environmental Health Science, Robert Stempel College of Public Health and Social Work, Florida International University, Miami, FL 33199, USA

[6]Department of Neuroscience, Mayo Clinic, Jacksonville, FL 32224, USA

[7]Center for Neuroimmunology and Glial Biology, Institute of Molecular Medicine, University of Texas Health Science Center at Houston, Houston, TX 77030, USA

[8]Lead contact

SUMMARY

Border-associated macrophages (BAMs) are tissue-resident macrophages that reside at the border of the central nervous system (CNS). Since BAMs originate from yolk sac progenitors that do not persist after birth, the means by which this population of cells is maintained is not well understood. Using two-photon microscopy and multiple lineage-tracing strategies, we determine that CCR2$^+$ monocytes are significant contributors to BAM populations following disruptions of CNS homeostasis in adult mice. After BAM depletion, while the residual BAMs possess partial self-repopulation capability, the CCR2$^+$ monocytes are a critical source of the repopulated BAMs. In addition, we demonstrate the existence of CCR2$^+$ monocyte-derived long-lived BAMs in a brain compression model and in a sepsis model after the initial disruption of homeostasis. Our study

*Correspondence: longjun.wu@uth.tmc.edu.

AUTHOR CONTRIBUTIONS

Conceptualization, L.W., J.Z., and L.-J.W.; methodology, L.W., J.Z., S.Z., and L.-J.W.; formal analysis, L.W.; investigation, L.W., J.Z., and S.Z.; resources, Y.W., M.W., and C.-Y.K.; data curation, L.W. and J.Z.; writing – original draft, L.W.; writing – review & editing, L.W., M.W., D.B.B., C.-Y.K., J.R.R., and L.-J.W.; visualization, L.W.; supervision, L.-J.W.; project administration, L.-J.W.; funding acquisition, L.-J.W. and J.R.R.

DECLARATION OF INTERESTS

The authors declare no competing interests.

SUPPLEMENTAL INFORMATION

Supplemental information can be found online at https://doi.org/10.1016/j.celrep.2024.114120.

reveals that the short-lived CCR2$^+$ monocytes transform into long-lived BAM-like cells at the CNS border and subsequently contribute to BAM populations.

In brief

In this study, Wang et al. demonstrate in mouse models that short-lived CCR2$^+$ monocytes engraft the brain border and transform into long-lived BAM (border-associated macrophage)-like cells to replenish the BAMs after acute depletion or in brain diseases where an initial loss of BAMs occurs, such as brain compression and meningitis.

Graphical Abstract

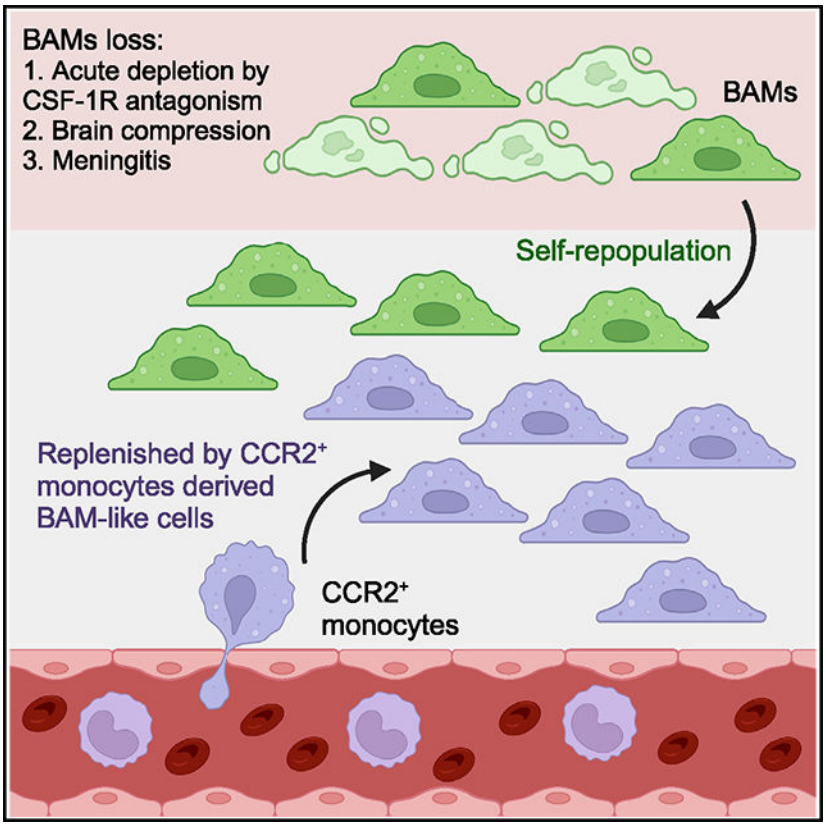

INTRODUCTION

The border of the central nervous system (CNS), which includes the dura mater, leptomeninges, choroid plexus, and perivascular space, harbors a unique immune population termed the CNS border-associated macrophages (BAMs).[1] Based on their anatomical locations, BAMs can be further classified into dura mater BAMs (dmBAMs), leptomeningeal BAMs (mBAMs), perivascular macrophages (PVMs), and choroid plexus BAMs (cpBAMs).[2] Of note, the mBAMs are the source for the PVMs postnatally; thus, both are termed subdural BAMs (sdBAMs).[3] In addition, BAMs have strikingly similar ontogeny to microglia, the CNS-resident macrophages in parenchyma,[4] in that both types of cells are developed from yolk sac erythromyeloid progenitors (EMPs) which cease to exist after

birth.[5–7] Thus, the means by which BAM populations are maintained and renewed have drawn increasing attention.[8]

Previous studies have reported that, under homeostatic conditions, sdBAMs are long-lived cells and assumed to be self-maintaining, while dmBAMs and cpBAMs are gradually renewed by cells of peripheral origin.[6,9] However, since CNS homeostasis and its border can be easily disrupted, often accompanied by loss of BAMs and infiltration of peripheral immune cells, the composition of BAM pools may also change. Thus, how BAMs are maintained and replenished within disease contexts is largely unexplored. Using two-photon microscopy, full-spectrum flow cytometry, and multiple lineage-tracing mouse models, we report the important contribution of $CCR2^{+}$ monocytes to BAM populations following disruption of CNS homeostasis.

RESULTS

BAMs are distinct immune populations at the CNS border

To initially characterize BAM populations, we started with the GEO: GSE128855 dataset, which contains single-cell RNA sequencing (scRNA-seq) data of all immune cells collected from the CNS and its border compartments.[9] The UMAP projection shows a clear separation of the BAMs cluster from the microglial cluster (Figure 1A). Next, we calculated BAM marker genes and selectively plotted the top eight, including *Ms4a7, Pf4, Mrc1, Igf1, Dab2, Cbr2, Folr2*, and *Mgl2* (Figure 1B). Despite the fact that the CD206 protein encoded by the Mrc1 gene has been widely used as the principal marker for BAMs,[6,7,10,11] we were concerned that it may not label the major histocompatibility complex (MHC) class $II^{low/negative}$ BAM populations.[9,12,13] Thus, we performed co-staining of CD206 with IBA1 and MHC class II and found a high efficiency of co-localization in both the MHC class II^{+} and MHC class II^{-} BAM populations (over 75%; Figures S1A–S1C). A few epiplexus cpBAMs could also be labeled by CD206 (Figure S1D), although the signal was weak, consistent with their low *Mrc1* transcription.[9] Thus, CD206 was used in the following histological experiments to identify BAMs in the current study.

Since BAMs reside in multiple interface compartments (Figure 1C), their morphology exhibited heterogeneity (Figure 1D). We used four shape descriptors (size, roundness, aspect ratio, and solidity) to briefly evaluate this heterogeneity (Figures S1E–S1H).[14] The results showed that dmBAMs are typically polarized, rod-shape cells with a higher aspect ratio. In contrast, mBAMs have the highest roundness index. PVMs are confined within the Virchow-Robin space along blood vessels, with no microglia-like processes. Compared to other BAMs, cpBAMs have more processes extended from somata, resulting in a decreased solidity index. These characteristic morphologies helped identify BAMs during the rest of the study.

BAMs are partially self-replenished after depletion

Previous studies have reported that sdBAMs are self-maintained with little contribution from peripheral immune cells until aging, while dmBAMs and cpBAMs are gradually replenished by cells from peripheral origin under homeostatic conditions.[6,9] We wondered

then whether BAMs can self-repopulate after depletion. To address this question, we utilized PLX3397, a CSF-1 receptor antagonist, to acutely deplete BAMs.[15–17] To genetically trace BAMs, we used the *Cx3cr1*$^{CreER/+}$*::R26*$^{tdTomato/+}$ mouse line, which labels BAMs, microglia, and a few circulating blood immune cells with tdTomato after tamoxifen injections. Since only BAMs and microglia are long-lived cells, while other CX3CR1^{+} immune cell types have comparably shorter life spans, a 4-week turnover period would leave only BAMs and microglia tdTomato^{+}.[9,18–22] We then fed mice PLX3397 chow for 5 weeks to deplete BAMs, followed by normal chow for 3 weeks to let BAMs repopulate (Figure 1E). Using two-photon *in vivo* imaging, we longitudinally monitored the depletion and repopulation of tdTomato^{+} dmBAMs and mBAMs, with intravenous (i.v.) injection of dextran-fluorescein isothiocyanate (FITC) to visualize blood vessels. If the tdTomato^{+} cell number in the meninges increased during repopulation, then it would suggest that dmBAMs and mBAMs are at least partially repopulated from residual BAMs. As expected, the number of tdTomato^{+} BAMs in the meninges gradually decreased after commencing PLX3397 chow and reached the minimum at depletion day 35. Interestingly, during repopulation, the number of tdTomato^{+} BAMs in the meninges increased (Figures 1E and 1F).

To rule out the possibility that the increased number of tdTomato^{+} cells during repopulation were due to the recently reported CreER leakiness issue,[23–25] we performed two-photon imaging of meningeal BAMs at repopulation day 2. We successfully captured the cell proliferation events of these tdTomato^{+} BAMs, suggesting that these resident BAM cells can self-repopulate (Figure S1I; Video S1). We also utilized flow cytometry to profile the repopulation process in the *Cx3cr1*$^{CreER/+}$*::R26*$^{tdTomato/+}$ mice (Figures S1J, S1K, and Figure S2). As expected, all repopulated microglia were tdTomato^{+} (Figures S1L and S1M), consistent with previous reports.[18] Around half of the overall repopulated BAMs were tdTomato^{+}, suggesting the partial self-repopulation of BAMs (Figures S1L and S1M). Together, these results indicate that BAMs can partially repopulate from residual BAMs that survived PLX3397 depletion.

CCR2^{+} monocytes are able to replenish BAMs after depletion

Interestingly, in addition to observing tdTomato^{+} BAMs during repopulation, we noticed sparse extravascular accumulation of dextran-FITC in tdTomato^{-} cells within the meninges by repopulation day 7 (Figure 1E, arrowhead; Figure 1G). To enhance the diffusion of dextran-FITC into the meninges for better visualization, we i.v. injected lower-molecular-weight dextran-FITC at repopulation day 10. An abundance of tdTomato^{-}FITC^{+} cells was observed in the meninges at repopulation days 14 and 21 (Figure 1E), whose morphology resembled dmBAMs and mBAMs (Figure 1H). In addition, the flow cytometry data also showed that the percentage of tdTomato^{+} cells in repopulated BAMs was significantly lower compared to the non-depletion control group, with the exception of the MHC class II^{lo}-cpBAMs group disturbed by an outlier (Figures S1L and S1M). This overall trend of decreased tdTomato^{+} BAMs after repopulation was consistent with a previous study using the *Cx3cr1*$^{CreER/+}$*::R26*$^{eYFP/+}$ mice with similar logic.[9] These data suggested that cells from peripheral origin could also replenish the BAM population.

Considering that CCR2^{+} monocytes are capable of infiltrating and transforming into tissue-resident macrophages in other organs,[26,27] we decided to investigate whether they could replenish PLX3397-depleted BAM pools. Therefore, we first used *Ccr2*$^{CreER/+}$*::R26*$^{DTR/+}$ mice to transiently trace CCR2^{+} monocytes. PLX3397 chow was provided for 4 weeks, and normal chow was supplied thereafter. Tamoxifen was injected on the last day of PLX3397 treatment and on the first day of normal chow supply to drive diphtheria toxin receptor (DTR) expression in CCR2^{+} monocytes (Figure 2A). If CCR2^{+} monocytes could replenish BAMs during repopulation, we hypostasized, then we would find DTR^{+}CD206^{+} BAMs; otherwise, only DTR^{-}CD206^{+} BAMs would exist (Figure 2B). We confirmed successful depletion of BAMs and microglia 4 weeks after PLX3397 supply (Figure S3A). Of note, DTR expression (determined by immunostaining) was not observed in the few surviving BAMs but was observed in small round cells, presumed to be monocytes (Figure S3B). Three weeks after repopulation, we found DTR^{+}CD206^{+} cells in all BAMs subtypes (Figure 2C). Specifically, more than 60% of all BAMs were DTR^{+}CD206^{+} (Figure 2D), demonstrating that CCR2^{+} monocytes have the capability to replenish a large percentage of the lost BAM populations.

We performed *in vivo* two-photon imaging to visualize the transformation of CCR2^{+} monocytes into dmBAMs and mBAMs during repopulation (Figure 2E). If monocytes transform into BAMs, then they will exhibit morphological changes, with increased cell area and aspect ratios and a decrease in solidity and roundness (Figure 2F). Indeed, we observed many small round CCR2^{+} monocytes accumulating along blood vessels at repopulation day 2, which gradually increased their size and polarity during repopulation (Figures 2G–2I). At repopulation day 28, we observed both dmBAM-like and mBAM-like cells at the meningeal level (Figure 2G, arrowhead). Under the control condition without depletion, we observed tdTomato^{+} BAMs in the meninges, suggesting their monocyte origin, but not the perivascular accumulation or subsequent transformation into BAMs, suggesting a very slow rate of monocyte-BAM transformation under homeostatic conditions (Figures S3C and S3D).

We also repeated the depletion-repopulation experiment in the *Ccr2*$^{CreER/+}$*::R26*$^{tdTomato/+}$ mice and conducted flow cytometry to study the frequency of tdTomato^{+} monocyte-derived BAMs (Figure 2J). Tamoxifen was injected on the last day of PLX3397 supply to transiently label a portion of CCR2^{+} monocytes. Tissues were collected at repopulation week 4, 8, and 12 or control week 8 for flow cytometry. A significant increase of tdTomato^{+} cells in the repopulated BAMs compared to control would suggest that CCR2^{+} monocytes can also replenish BAMs (Figure 2K). Indeed, the flow cytometry results showed a significant increase of tdTomato^{+} BAMs at different repopulation time points compared to control week 8 (Figure 2L). Since monocytes can slowly engraft the dura mater and choroid plexus to become MHC class II^{hi} BAMs,[9] we examined the percentage of MHC class II^{hi} cells in tdTomato^{+} BAMs. All tdTomato^{+} BAM subtypes in the control group showed a high percentage of MHC class II^{hi}, indicating their monocyte origin (Figure 2M). Interestingly, both the repopulated tdTomato^{+} dmBAMs and tdTomato^{+} sdBAMs, but not tdTomato^{+} cpBAMs, showed decreased percentages of MHC class II^{hi} cells compared to the control (Figure 2M). We present the tSNE plots to show the tdTomato expression of microglia and BAM subtypes from control and repopulation week 8 (Figure 2N). We also performed

immunostaining of the BAM marker CD206. Our results show that CD206$^+$tdTomato$^+$ cells exhibited typical BAM morphology at repopulation week 8 (Figure S3E). Together, these results indicate that CCR2$^+$ monocytes significantly replenish the BAM population after their depletion.

Microglia do not contribute to BAM repopulation

Since both BAMs and microglia develop from the same progenitors,[7,28] and because microglia have a strong capacity for selfrenewal,[18] we wanted to know whether microglia could also contribute to BAM repopulation. Thus, we used *Tmem119-CreER::R26*$^{tdTomato/+}$ mice to specifically label microglia (Figure S4A). If any tdTomato$^+$CD206$^+$ BAMs existed after repopulation, then it would indicate contributions from microglia (Figure S4B). We observed a tracing efficiency of approximately 94% in the cortex, 88.67% in the hippocampus, and 69.67% in the cerebellum for parenchymal IBA1$^+$ microglia (Figures S4C and S4E). In addition, we found no tdTomato$^+$ dmBAMs, mBAMs, or PVMs, while around 7% of cpBAMs displayed tdTomato expression (Figures S4D and S4F), supposed to be the epiplexus (Kolmer) cells that exhibit microglia marker genes.[9] After BAM depletion and repopulation, we found no tdTomato$^+$CD206$^+$ BAMs in the dura mater, leptomeninges, or perivascular spaces. Approximately 8% of CD206$^+$ cpBAMs were tdTomato$^+$, comparable with what was observed before depletion (Figures S4G and S4H). This is consistent with a previous study showing total self-repopulation of the epiplexus cpBAMs.[9] Of note, we observed a large quantity of tdTomato$^+$ fibroblast-like cells in the dura mater and a sparse few along the leptomeninges and vessel walls (Figures S4D and S4G) that were PDGFRα$^+$ (Figure S4I). Our results indicated that microglia do not contribute to BAM repopulation.

Single-cell transcriptomics reveal close association of CCR2$^+$ monocytes with BAMs

To understand the transcriptional similarity between BAMs, monocytes, and microglia, we utilize the GEO: GSE128855 dataset to calculate the correlation of their transcriptome profiles. We found that monocytes and BAMs had the most correlated transcriptome profiles, while monocytes and microglia had the least correlated profiles (Figure S5A, top left). Although both the microglia and BAMs are tissue-resident macrophages, their transcriptomic similarity was lower than that between the BAMs and monocytes. We also found that all correlations were high between monocytes and BAMs isolated from the same region (all higher than 0.57; Figure S5A, bottom right).

We also investigated the GEO: GSE118948 dataset, which sequenced CD45$^+$ cells isolated from the meninges, choroid plexus, brain parenchyma, and peripheral blood.[29] We found that monocytes were clearly separated into two subclusters (Figures S5B and S5C). Wondering whether this separation was due to the differences in location from which these monocytes were collected (i.e., brain vs. blood), we labeled each cell with its tissue collection location as reported in the original study. Surprisingly, we found that monocyte cluster 1 contained monocytes collected from all CNS locations and blood, while monocyte cluster 2 contained mostly blood monocytes (Figures S5D and S5E). We found that monocyte subcluster 1 was *Ly6-c2*^{Hi}*Ccr2*^{Hi}*Sell*^{Hi}*Spn*^{Low}*Treml4*^{Low}, resembling the classical monocytes, while monocyte subcluster 2 was *Ly6c2*^{Low}*Ccr2*^{Low} *Sell*^{Low}*Spn*^{Hi}*Treml4*^{Hi},

resembling non-classical monocytes[27] (Figures S5F), which highlighted the close relationship of CCR2^{+} monocytes to the CNS border.

The higher correlation between monocytes and BAMs made us hypothesize that there was an intermediate cell state when CCR2^{+} monocytes transformed into mature BAMs, similar to the classical monocyte-derived cells described in a previous study.[9] To test this idea, we used the GEO: GSE150169 dataset,[30] which contained CD11b-sorted brain immune cells from BAM deletion day 14, repopulation day 2, and control conditions (Figure 3A), highly relevant to our depletion-repopulation experiments. Clusters were annotated by their marker genes (Figures 3B; S4G). A deeper characterization of the BAM/monocyte/dendritic cells cluster yielded 5 populations: *Ccr2*^{lo} non-classical monocytes (ncMonocytes), *Ccr2*^{hi} classical monocytes (cMonocytes), *Ccr2*^{hi} classical monocyte-derived cells (cMdCs), dendritic cells (DCs), and MHC class II^{lo} BAMs (Figures 3C; S4H). As expected, we found a dramatic loss of both the MHC class II^{lo} BAMs and a portion of cMdCs after depletion by PLX5622, which had high *Csf1r* expression (Figures 3D and 3E). We performed the SCORPIUS trajectory analysis[31,32] of cMonocytes, cMdCs, and MHC class II^{lo} BAMs, and found that the cMdC automatically clustered between cMonocytes and MHC class II^{lo} BAMs (Figure 3F). We calculated the gene modules involved in this transformation, which showed transcriptional gradients that were lost or gained as cells moved from classical monocytes to BAMs (Figure 3G). The gene modules were strikingly similar to the previous study,[9] showing the gradient loss of *Ccr2* and *Ly6c2* and gain of BAMs marker genes such as *Aif1, Mrc1, Apoe*, and *Pf4*. We then examined the gene expression of these three populations at different time points. We found that both cMonocytes and cMdCs had high *Ccr2* expression at the end of the PLX5622 depletion and repopulation day 2 (Figures 3H and 3I), which could be well targeted in our lineage-tracing *Ccr2*$^{CreER/+}$*::R26*$^{tdTomato/+}$ mice. Interestingly, at repopulation day 2, there was an increased portion of CCR2^{hi}MHC class II$^{lo/neg}$ cMdC population (Figures 3J and 3K). This could either indicate the increased transformation of cMonocytes to cMdCs during the early repopulation phase, where many cMonocytes have not yet express MHC class II, or the interesting possibility that these CCR2^{+}MHC class II^{-} cMdCs may directly transform into MHC class II^{lo} BAMs. Overall, these scRNA-seq data suggest the transformation of CCR2^{+} monocytes and their derived cells during early repopulation.

CCR2^{+} monocytes replenish BAMs following disease-induced BAMs loss

Since PLX3397-mediated BAM depletion is an extreme situation, we asked whether CCR2^{+} monocytes could contribute to BAM populations under disease conditions with an initial BAM loss. Therefore, we utilized a brain compression model and a sepsis model to address this question. The brain compression model was induced by compressing the cortex with a cover glass during two-photon cranial window surgery (Figure S6A). We observed the formation of characteristic honeycomb and jellyfish structures by microglia in the cortex of the *Cx3cr1*$^{Gfp/+}$ mice in response to injury (Figure S6B; Video S2), similar to a previous report.[33] Interestingly, time-lapse *in vivo* two-photon imaging showed a rapid loss of both dmBAMs and mBAMs within the first hour of compression (Figure 4A, arrowhead). We then observed an increased number of GFP^{+} cells in the meninges during the subsequent weeks, whose morphology gradually resembled dmBAMs and mBAMs by

3 months (Figure 4A, arrowhead). The initial loss of BAMs was confirmed by CD206 immunostaining 3 h after the compression (Figures S6C and S6D). We then asked whether CCR2$^+$ monocytes contributed to the replenishment of BAMs. To this end, we performed brain compression in *Ccr2*$^{CreER/+}$*::Rosa26*$^{tdTomato/+}$ mice and longitudinally monitored CCR2$^+$ monocyte response (Figure 4B). Indeed, we observed infiltration of a significant number of small round tdTomato$^+$ monocytes into the meninges 1 day after injury (Figure 4B). We further observed that these tdTomato$^+$ monocytes gradually transformed their morphology throughout injury onset and recovery (Figure 4B). By 3 months, tdTomato$^+$ cells exhibited dmBAM-like and mBAM-like morphology (Figure 4B, arrowhead). We collected tissue and performed immunostaining to quantify tdTomato$^+$CD206$^+$ cell number and found that approximately 70.66% dmBAMs and 52.15% mBAMs were tdTomato$^+$ in the compressed region, while only 10.39% dmBAMs and 5.66% mBAMs were tdTomato$^+$ in the non-compressed region (Figures 4C and 4D). We also performed flow cytometry on cells collected from compression regions or sham procedure regions 12 weeks after surgery (Figure S6G). The compression region had a higher ratio of both MHC class II^{hi} dmBAMs and MHC class II^{hi} sdBAMs, suggesting the increase of monocyte-derived BAMs in response to brain compression (Figure S6H). The frequencies of tdTomato$^+$ dmBAM and tdTomato$^+$ sdBAMs were also increased in the compression region compared to the sham group (Figure S6I). Interestingly, compared with tdTomato$^+$ sdBAMs in the sham group, we found a decreased frequency of tdTomato$^+$MHC class II^{hi} sdBAMs in the compression region (Figure S6J). A similar trend was also observed in the dmBAMs, but due to the limited animal numbers, we could not detect a difference (Figure S6J).

To further study CCR2$^+$ monocytes in replenishing BAM populations, we used a sepsis model that induces severe systemic inflammation and meningitis via i.v. injection of lipopolysaccharide (LPS; 2.5 mg/kg i.v.). High-dose LPS is known to disrupt homeostasis in the CNS and its border compartments and induce macrophage apoptosis.[34,35] We observed a decreased number of dmBAMs in the LPS group compared to the PBS control (Figures S6E and S6F). Next, we labeled CCR2$^+$ monocytes in *Ccr2*$^{CreER/+}$*::Rosa26*$^{tdTomato/+}$ mice and examined their incorporation into BAM populations (Figure 4E). We collected tissue at 8 weeks post LPS or PBS injection and found a mixture of tdTomato$^+$CD206$^+$ and tdTomato$^-$CD206$^+$ BAMs (Figure 4F). The ratio of tdTomato$^+$CD206$^+$ dmBAMs, mBAMs, and cpBAMs in the LPS group was significantly higher than in the PBS group (Figure 4G). Together, our results demonstrate that, in addition to BAM self-repopulation, the CCR2$^+$ monocytes are able to infiltrate into the diseased brain and transform into long-living BAM-like cells that replenish the lost BAM populations (Figure 4H).

DISCUSSION

Recent studies using parabiosis and the constitutive FLT3^{Cre} tracing line have reported that, under homeostatic conditions, sdBAMs maintain their embryo ontogeny with little contribution from peripheral progenitors until aging, while dmBAMs and cpBAMs are slowly replaced by cells derived from peripheral circulation.[6,9] However, it would be interesting to perform the depletion-repopulation experiment in the FLT3^{Cre} tracing line to investigate the contribution of bone marrow progenitor-derived cells, most likely CCR2$^+$ monocytes, to the replenished BAM population. The infiltration of CCR2$^+$ monocytes

into the CNS and its border has been documented in a broad spectrum of diseases, such as seizures,[36–38] pain,[22,39] Alzheimer's disease,[40–42] ischemic and hemorrhagic stroke,[43–46] traumatic brain injury,[47] and meningitis.[48,49] Recent studies using the Ccr2-CreER lineage-tracing mouse line have shown convincing evidence of long-term engraftment and transformation of infiltrated monocytes into microglia-like cells in the brain parenchyma following brain irradiation and stroke.[45,50] In this study, we demonstrate that $CCR2^+$ monocytes replenish the BAM population in three animal models that have an initial loss of BAMs. Of note, a subtype of cpBAMs (namely, epiplexus cpBAMs or Kolmer cells)[51] are reported to express multiple microglial marker genes, such as *P2ry12* and *Sall1*, and can totally self-repopulate after depletion.[9] Indeed, we found some $tdTomato^+$ cpBAMs in the *Tmem119-CreER::R26*$^{tdTomato/+}$ mouse, likely Kolmer cells, whose ratio remained the same between control and repopulation conditions.

Trafficking of circulating monocytes are highly regulated. The CCR2 receptor is critical for the egress of classical monocytes from the bone marrow[52,53] and for infiltration into the CNS.[26] Multiple ligands for CCR2, such as CCL2, CCL7, CCL12 (mouse only), and CCL13 (human only), have been reported to play critical roles in driving monocyte infiltration into the CNS,[54–57] likely in a disease-dependent manner. CCL2 is expressed by a variety of cells in the CNS and its border, such as neurons, astrocytes, microglia, smooth muscle cells, endothelial cells, and fibroblasts.[58–61] CCL7 is expressed by astrocytes,[62] CCL12 by microglia,[63] and CCL13 by inflamed human brain blood vessels.[64] The extravasation of monocytes can be facilitated by the fenestrated endothelia in the dura mater and choroid plexus vasculatures. Despite the endothelia in leptomeningeal blood vessels being connected by tight junctions under homeostasis, it can be disrupted after disease.[65–67] Additionally, a recent discovery of the mesothelium structure in the leptomeninges, termed the subarachnoid lymphatic-like membrane, suggests the existence of a myeloid cell hub within the leptomeninges that possibly provides a novel route for monocyte infiltration into the leptomeninges.[68] Multiple molecules may orchestrate the transformation from monocytes to BAMs, such as interferon regulatory factor 8 and MAF bZIP transcription factor B, deficiency of which will impede BAM expansion.[6] In addition, the integrin signaling pathways are critical for PVMs to expand from mBAMs and descend into the Virchow-Robin γ is reported to drive monocyte differentiation after engraftment in the dura mater within a murine viral meningitis model.[49] However, it still remains unknown whether the replenishment of BAMs by $CCR2^+$ monocytes is regulated by similar molecular mechanisms.

We believe that the empty niche created by the initial loss of BAMs is important for the long-term engraftment of monocyte-derived BAMs. A massive loss of the BAMs in the diseased brain is not uncommon. Meningitis caused by bacterial, virus, and parasite infection is a relevant clinical disease that can result in BAM loss.[69] Gram-negative meningococci, such as *Neisseria meningitidis*, are one of the major causes of bacterial meningitis.[70] The LPS on the outer membrane of these meningococcus functions as an endotoxin and virulence factor,[71] which can be recognized by macrophage Toll-like receptor 4.[72] The deleterious effects of LPS trigger excessive production of nitric oxide by macrophages, which can eventually lead to macrophage apoptosis.[35] In addition, a virus infection induces massive loss of BAMs and subsequent long-term engraftment of $CCR2^+$

monocytes in the meninges have been reported in a murine viral meningitis model.[49] Interestingly, a previous study on the parasite *Trypanosoma brucei*-induced meningitis reported different results to our LPS study.[73] This study reported the existence of monocyte-derived dmBAMs and cpBAMs upon parasitic meningitis resolution but not monocyte-derived sdBAMs.[73] This could possibly be explained by the different disease settings. In our model, we used a high LPS dose to acutely induce severe systemic inflammation that caused BAMs loss. In the *T. brucei* meningitis model, the parasites gradually accumulated in the CNS-border compartments in weeks. In addition, the parasitemia peaked in the leptomeninges was also less severe compared to the dura mater and choroid plexus in the model, which might not cause sdBAM loss, and, thus, no empty niche was created. Actually, we think a possibly better disease model to mimic the BAM loss and monocyte replenishment scenario would be the attenuated lymphocytic choriomeningitis virus (r3LCMV) model reported previously,[49] where the virus can directly infect BAMs and cause their loss, while the fatality rate of the host is low.

Limitations of the study

There are several limitations of the current study. First, in the brain compression flow cytometry experiment, we did not evaluate the absolute quantity of the MHC class II^{hi} and MHC class II^{lo} BAMs at 12 weeks post compression. The increased frequency of $CCR2^{+}$ monocyte-derived BAMs might be due to the increased absolute number of the MHC class II^{hi} BAMs, while the number of MHC class II^{lo} BAMs remain unchanged. Second, we did not investigate whether the monocyte-derived BAM-like cells will eventually become indistinguishable from naive BAMs upon disease resolution, both numerically and functionally. To possibly address this question, scRNA-seq of monocyte-replenished BAMs and naive BAMs at multiple time points after disease resolution would be of interest for future studies.

In summary, we demonstrated the capability of $CCR2^{+}$ monocytes to replenish the BAM populations in the diseased brain. Future studies are needed to understand what molecular signals drive monocyte transformation into MHC class II^{hi} and MHC class II^{lo} BAMs and how monocyte-derived BAMs can be harnessed to treat disease conditions like traumatic brain injury or meningitis.

STAR★METHODS

RESOURCE AVAILABILITY

Lead contact—Further information and requests for resources and reagents should be directed to and will be fulfilled by the lead contact, Dr. Long-Jun Wu (longjun.wu@uth.tmc.edu).

Materials availability—This study did not generate new unique reagents or materials.

Data and code availability

- Single-cell RNA-seq data analyzed in this study are publicly available at GEO. Accession numbers are listed in the key resources table. Other data reported in this paper will be shared by the lead contact upon request
- All codes for the single-cell RNA-seq data analysis have been deposited at Zenodo and is publicly available as of the date of publication by https://doi.org/10.5281/zenodo.10836098. Link to files is listed in the key resources table.
- Any additional information required to reanalyze the data reported in this paper is available from the lead contact upon request.

EXPERIMENTAL MODEL AND STUDY PARTICIPANT DETAILS

Animals—The Mayo Clinic Institutional Animal Care and Use Committees (IACUC) approved all procedures utilized within this study. Adult mice of both sexes were used between 6 weeks and 6 months of age. No differences were noted between male and female mice so data was combined. Mice of the same sex and genotype were randomly assigned to experimental groups. Homozygous CX3CR1-CreER mice (JAX:020940), Tmem119-CreER mice (JAX:031820), two strains of CCR2-CreER mice (the first strain was kindly provided by Dr. Chia-Yi Kuan, University of Virginia; the second strain is JAX:035229), were crossed with homozygous Rosa26-tdTomato (JAX:007914) or Rosa26-iDTR (JAX:007900) mice to generate $CX3CR1^{CreER/+}$:$R26^{tdTomato/+}$ mice, $Tmem119^{CreER/+}$:$R26^{tdTomato/+}$ mice, $CCR2^{CreER/+}$:$R26^{tdTomato/+}$, and $CCR2^{CreER/+}$:$R26^{iDTR/+}$ mice, respectively. Mice were group housed on a 12-h light/dark cycle and in a climate-controlled environment. Food and water were provided *ad libitum*.

METHOD DETAILS

Immunofluorescence staining—Mice were deeply anesthetized with isoflurane and then transcardially perfused with ice-cold phosphate-buffered saline (PBS) followed by 4% paraformaldehyde (PFA) in PBS. The whole brain and skull were harvested and post-fixed in 4% PFA overnight at 4 °C. The dura mater was gently peeled from skull, leptomeninges were gently harvested from the brain surface, and choroid plexus were collected from the lateral ventricles and 4^{th} ventricles.[76] Post-fixed brains were dehydrated with a 30% sucrose solution for 2 days before cryosection. Free-floating immunostaining was used. Briefly, sections were washed 3 times with tris-buffered saline (TBS) then blocked with 5% goat or donkey serum in TBS containing 0.4% Triton X-100 at room temperature for 1 h. Sections were then incubated with primary antibodies (Rat anti Mouse CD206, BIO-RAD, MCA2235, 1:100; Goat anti Mouse CD206, R&D, AF2535, 1:500; Goat anti Human DTR, R&D, AF-259-NA, 1:300; Rat anti Mouse CD31, BD BIOSCIENCE, 550274, 1:50; Goat anti Mouse CD31, NOVUS BIOLOGICALS, AF3628, 1:300; Rat anti Mouse MHCII, Invitrogen, 14–5321-82, 1:200, Rabbit anti Mouse IBA1, Abcam, AB178847; Rabbit anti Mouse PDGFRa, AB203491, 1:200) diluted in 1% goat or donkey serum in the TBS at 4°C overnight. Sections were then washed with TBS 3 times and incubated with goat or donkey secondary antibodies (1:500, Alexa Fluor 488/555/594/647 anti-rat, or anti-goat, A11055, A21434, A11058, A21247, and A21447) for 1 h at room temperature. To label blood

vessel, some sections were incubated with Lectin (LEL, TL) DyLight 594 (1:150, Vector Lab, DL-1177–1) for 1 h at room temperature. Sections were then washed and mounted with DAPI Fluoromount-G mounting medium (Southern Biotech). Fluorescent images were captured by confocal microscope (LSM 980, Zeiss) and processed with ImageJ[75] (National Institutes of Health).

Tamoxifen injection—*CX3CR1*$^{CreER/+}$*::R26*$^{tdTomato/+}$ and *Tmem119*$^{CreER/+}$*::R26*$^{tdTomato/+}$ mice were *i.p.* injected 100 mL tamoxifen solution (20 mg/ml) every 2 days for a total of 3 injections to induce Cre recombinase activity. *CCR2*$^{CreER/+}$*::R26*$^{iDTR/+}$ and *CCR2*$^{CreER/+}$*::R26*$^{tdTomato/+}$ mice in the BAM depletion and repopulation histology experiments were *i.p.* injected with 100 μL tamoxifen solution (20 mg/ml) on the last day of PLX3397 supply and the first day of normal chow supply for a total of 2 injections. *CCR2*$^{CreER/+}$*::R26*$^{tdTomato/+}$ mice in the BAM depletion and repopulation flow cytometry experiments were only *i.p.* injected with 100 μL tamoxifen solution (20 mg/ml) on the last day of PLX3397 supply, which is a very conservative strategy to transiently label a portion of CCR2^{+} monocytes. *CCR2*$^{CreER/+}$*:: R26*$^{tdTomato/+}$ mice in the brain compression and sepsis model experiments were *i.p.* injected 100 mL tamoxifen solution (20 mg/ml) 1 day before disease induction.

BAMs and microglia depletion—Chow containing colony-stimulating factor 1 receptor (CSF1R) inhibitor PLX3397 (600 mg/kg, Chemgood) was provided *ad libitum* at least for 4 weeks before experiments. Successful BAM depletion was confirmed by either immunostaining or two-photon imaging.

Two-photon imaging—Mice were deeply anesthetized with isoflurane (5% for induction; 1.5% for maintenance and surgery). After shaving the skin hair on the head, the mouse head was fixed with a stereotactic frame and cleaned with 3 alternating applications of betadine and 70% alcohol, after which lubricating eye ointment was applied. Temperature was maintained by a heating pad during surgery. The scalp was cut to expose the skull. The connective tissue on skull surface was cleared using 3% hydrogen peroxide (McKesson, #23-D0012), and a circular 3-mm-diameter window was gently drilled open using a dental drill (Osada Model EXLM40). The skull flap was gently removed by forceps. Windows were placed above the somatosensory cortex such that the skull was removed with the center at about 2.5 posterior and ± 2mm lateral to bregma. The exposed dura mater was kept moist with sterile saline. A sterilized 4-mm glass coverslip (Warner Instruments) was glued onto the skull over the expose brain region by dental glue (Ivoclar, Tetric EvoFlow, 595954WW), avoiding direct compression of brain surface. The rest of the skull was first covered with iBond Total Etch glue (Kulzer) and the dental glue, both cured with a LED blue light. Finally, a four-point head plate (NeuroTar) was secured over the window with dental glue. This craniotomy procedure were also described in our previous studies.[77,78] Following this surgery, mice were either immediately transferred to the two-photon microscope for acute imaging or returned to home cage after recovery from anesthesia. For chronic imaging, mice were allowed to recover from the surgery for at least 4 weeks. Mice that showed a loss in imaging window clarity during the period of observation were excluded from the study.

All two-photon *in vivo* imaging procedures were performed at room temperature. Mice were anesthetized with isoflurane (5% for induction; 1% for maintenance) and fixed under the two-photon microscope via the affixed head plate. Dextran was *i.v.* injected (50μL 5 mg/ml 70kMW Dextran-FITC for vessel labeling, 100uL 25 mg/ml 10kMW Dextran-FITC to boost diffusion into meninges) before imaging. FITC/eGFP and tdTomato signal was captured by a multiphoton microscope (Scientifica) equipped with a Mai-Tai DeepSee laser (Spectra Physics) tuned to 940 nm with a 40x water immersion lens (Nikon). Images were collected at a 1024 × 1024-pixel resolution.

Single cell RNA sequencing analysis—Single cell RNA sequencing files containing all the immune cells collected in the CNS and its border compartments was downloaded from the Gene Expression Omnibus (GEO) under accession number GSE128855. The Seurat package was used for analysis.[74] In brief, a Seurat object was created from the feature-barcode matrices and was annotated by the metadata files provided by the original study. After filtering out low-quality reads, the expression matrices were normalized with a scale factor of 1e6 and scaled. Linear dimension reduction was done via principal component analysis (PCA). UMAP projection was done using the DimPlot function. BAM marker genes were calculated with the FindMarkers function. Selected top BAM marker genes were plotted with the VlnPlot function. Correlation of gene expressions among different cell clusters was performed with the cor function in the stats R package.

Single cell RNA sequencing files containing $CD45^+$ immune cells from meninges, choroid plexus, CNS parenchyma, and peripheral blood was downloaded from GEO under accession number GSE118948. Only cells collected in the naive condition were used for analysis. After filtering out the low-quality reads, expression matrices were normalized with a scale factor of 1e6 and scaled. Cell identity was identified according to the marker genes used in the original study. Microglia, monocytes, and BAMs were then subset out. tSNE plot was done by DimPlot function. Gene expression heatmap was done with the FeaturePlot function.

Single cell RNA sequencing files containing $CD11b^+$ cells from whole brain were downloaded from GEO under accession number GSE150169. After filtering out the low-quality reads, expression matrices were normalized with a scale factor of 1e6 and scaled. Cell identity was identified according to the marker genes shown in the supplementary figure. Trajectory inference was done by SCORPIUS package.[32] UMAP plot was done by DimPlot function. Gene expression heatmap was done with the FeaturePlot function. Violin plots was done by VlnPlot function.

Spectrum flow cytometry—Spectrum flow cytometry was conducted to assess the frequency of $tdTomato^+$ BAMs.[79,80] Mice were euthanized and intracardiac perfused with cold PBS to remove blood. Dura mater, enriched cortex, and choroid plexus were collected, and single cell suspension was prepared according to the published protocol.[76] Single cell suspensions incubated with a combination of the following antibodies along with a Fc blocking antibody: Ghost Dye Red 780 (1:1 000, Tonbo Biosciences, 13–0865), APC/Fire810 anti-NK1.1 (1:100, BioLegend, 156519), BB700 anti-MHC II (1:500, BD Biosciences, 746197), APC anti-Ly6G (1:100, BD Biosciences, 560599), PE-CF594 anti-

CD45 (1:1000, BD Biosciences, 562420), PE-Cy5 anti-CD11b (1:1000, Tonbo Biosciences, 55–0112-U100), PE-Cy7 anti-TCRβ (1:100, Biolegend, 109221), Spark NIR 685 anti-B220 (1:200, BioLegend, 103267).

Samples were then assessed by the spectral flow cytometer (Cytek Aurora, Cytek Biosciences) equipped with SpectroFlo software (Cytek Biosciences). Acquired files were then analyzed by FlowJo software (BD Life Sciences).

Mild brain compression model—A modified craniotomy procedure for two-photon imaging was used to cause mild-brain compression. A 5~6mm diameter circular cranial window, instead of 3mm, was drilled open. A sterilized 5-mm glass coverslip (Warner Instruments) was then place directly onto the dura mater, firmly compressing the brain cortex. No bleeding or obvious cortical trauma shall be induced by this procedure. The coverslip was secured by dental glue onto the skull. Mice were immediately transferred to the two-photon microscope for acute imaging following the surgery.

LPS-induced sepsis model—To acutely induce sepsis and systemic inflammation, adult $CCR2^{CreER/+}::R26^{tdTomato/+}$ mice were *i.v.* injected Lipopolysaccharides (2.5 mg/kg, Sigma-Aldrich, L2880) and returned to a clean home cage. Nutritional gel food was provided to facilitate recovery.

QUANTIFICATION AND STATISTICAL ANALYSIS

Image analysis—For cell morphology analysis, the ROI of each cell shape was manually drawn with the *Freehand Selection* in the ImageJ.[75] The analysis parameters including *Area* and *Shape Descriptors* were selected in the *Set Measurements* menu. Cell counts were performed manually in all histological studies.

Statistics—Statistical details for each specific experiment are described in each figure legend. Unpaired t test was used for statistical comparison of most experiments with 2 groups. Paired t test was used in the brain compression model comparing the compression region and non-compression region from the same mouse. When comparing more than 2 groups, one-way ANOVA with Turkey's multiple comparisons test was used for post-hoc analysis. We didn't use methods to determine whether the data met assumptions of the statistical approach. Results are presented as mean ± standard error of the mean (SEM). Statistical significance was determined by $p < 0.05$. Statistical analyses were conducted using GraphPad Prism 8 software.

Supplementary Material

Refer to Web version on PubMed Central for supplementary material.

ACKNOWLEDGMENTS

We thank members and collaborators of the Wu lab for insightful discussions. This work was supported by the following grants from the National Institutes of Health: R35NS132326 (to L.-J.W.) and R01ES033892 (to J.R.R. and L.-J.W.).

REFERENCES

1. Herz J, Filiano AJ, Wiltbank AT, Yogev N, and Kipnis J (2017). Myeloid Cells in the Central Nervous System. Immunity 46, 943–956. 10.1016/j.immuni.2017.06.007. [PubMed: 28636961]
2. Kierdorf K, Masuda T, Jordão MJC, and Prinz M (2019). Macrophages at CNS interfaces: ontogeny and function in health and disease. Nat. Rev. Neurosci. 20, 547–562. 10.1038/s41583-019-0201-x. [PubMed: 31358892]
3. Masuda T, Amann L, Monaco G, Sankowski R, Staszewski O, Krueger M, Del Gaudio F, He L, Paterson N, Nent E, et al. (2022). Specification of CNS macrophage subsets occurs postnatally in defined niches. Nature 604, 740–748. 10.1038/s41586-022-04596-2. [PubMed: 35444273]
4. Prinz M, Jung S, and Priller J (2019). Microglia Biology: One Century of Evolving Concepts. Cell 179, 292–311. 10.1016/j.cell.2019.08.053. [PubMed: 31585077]
5. Davies LC, Jenkins SJ, Allen JE, and Taylor PR (2013). Tissue-resident macrophages. Nat. Immunol. 14, 986–995. 10.1038/ni.2705. [PubMed: 24048120]
6. Goldmann T, Wieghofer P, Jordão MJC, Prutek F, Hagemeyer N, Frenzel K, Amann L, Staszewski O, Kierdorf K, Krueger M, et al. (2016). Origin, fate and dynamics of macrophages at central nervous system interfaces. Nat. Immunol. 17, 797–805. 10.1038/ni.3423. [PubMed: 27135602]
7. Utz SG, See P, Mildenberger W, Thion MS, Silvin A, Lutz M, Ingelfinger F, Rayan NA, Lelios I, Buttgereit A, et al. (2020). Early Fate Defines Microglia and Non-parenchymal Brain Macrophage Development. Cell 181, 557–573.e18. 10.1016/j.cell.2020.03.021. [PubMed: 32259484]
8. Prinz M, Masuda T, Wheeler MA, and Quintana FJ (2021). Microglia and Central Nervous System-Associated Macrophages-From Origin to Disease Modulation. Annu. Rev. Immunol. 39, 251–277. 10.1146/annurev-immunol-093019-110159. [PubMed: 33556248]
9. Van Hove H, Martens L, Scheyltjens I, De Vlaminck K, Pombo Antunes AR, De Prijck S, Vandamme N, De Schepper S, Van Isterdael G, Scott CL, et al. (2019). A single-cell atlas of mouse brain macrophages reveals unique transcriptional identities shaped by ontogeny and tissue environment. Nat. Neurosci. 22, 1021–1035. 10.1038/s41593-019-0393-4. [PubMed: 31061494]
10. Brioschi S, Belk JA, Peng V, Molgora M, Rodrigues PF, Nguyen KM, Wang S, Du S, Wang WL, Grajales-Reyes GE, et al. (2023). A Cre-deleter specific for embryo-derived brain macrophages reveals distinct features of microglia and border macrophages. Immunity 56, 1027–1045.e8. 10.1016/j.immuni.2023.01.028. [PubMed: 36791722]
11. Wu X, Saito T, Saido TC, Barron AM, and Ruedl C (2021). Microglia and CD206(+) border-associated mouse macrophages maintain their embryonic origin during Alzheimer's disease. Elife 10, e71879. 10.7554/eLife.71879. [PubMed: 34609281]
12. Mrdjen D, Pavlovic A, Hartmann FJ, Schreiner B, Utz SG, Leung BP, Lelios I, Heppner FL, Kipnis J, Merkler D, et al. (2018). HighDimensional Single-Cell Mapping of Central Nervous System Immune Cells Reveals Distinct Myeloid Subsets in Health, Aging, and Disease. Immunity 48, 380–395.e6. 10.1016/j.immuni.2018.01.011. [PubMed: 29426702]
13. Rebejac J, Eme-Scolan E, Arnaud Paroutaud L, Kharbouche S, Teleman M, Spinelli L, Gallo E, Roussel-Queval A, Zarubica A, Sansoni A, et al. (2022). Meningeal macrophages protect against viral neuroinfection. Immunity 55, 2103–2117.e10. 10.1016/j.immuni.2022.10.005. [PubMed: 36323311]
14. Schindelin J, Arganda-Carreras I, Frise E, Kaynig V, Longair M, Pietzsch T, Preibisch S, Rueden C, Saalfeld S, Schmid B, et al. (2012). Fiji: an open-source platform for biological-image analysis. Nat. Methods 9, 676–682. 10.1038/nmeth.2019. [PubMed: 22743772]
15. Green KN, Crapser JD, and Hohsfield LA (2020). To Kill a Microglia: A Case for CSF1R Inhibitors. Trends Immunol. 41, 771–784. 10.1016/j.it.2020.07.001. [PubMed: 32792173]
16. Elmore MRP, Najafi AR, Koike MA, Dagher NN, Spangenberg EE, Rice RA, Kitazawa M, Matusow B, Nguyen H, West BL, and Green KN (2014). Colony-stimulating factor 1 receptor signaling is necessary for microglia viability, unmasking a microglia progenitor cell in the adult brain. Neuron 82, 380–397. 10.1016/j.neuron.2014.02.040. [PubMed: 24742461]
17. Spangenberg E, Severson PL, Hohsfield LA, Crapser J, Zhang J, Burton EA, Zhang Y, Spevak W, Lin J, Phan NY, et al. (2019). Sustained microglial depletion with CSF1R inhibitor impairs

parenchymal plaque development in an Alzheimer's disease model. Nat. Commun. 10, 3758. 10.1038/s41467-019-11674-z. [PubMed: 31434879]

18. Huang Y, Xu Z, Xiong S, Sun F, Qin G, Hu G, Wang J, Zhao L, Liang YX, Wu T, et al. (2018). Repopulated microglia are solely derived from the proliferation of residual microglia after acute depletion. Nat. Neurosci. 21, 530–540. 10.1038/s41593-018-0090-8. [PubMed: 29472620]
19. Tay TL, Mai D, Dautzenberg J, Fernández-Klett F, Lin G, Sagar Datta, M., Drougard A., Stempfl T., Ardura-Fabregat A., et al. (2017). A new fate mapping system reveals context-dependent random or clonal expansion of microglia. Nat. Neurosci. 20, 793–803. 10.1038/nn.4547. [PubMed: 28414331]
20. Mildner A, Schmidt H, Nitsche M, Merkler D, Hanisch UK, Mack M, Heikenwalder M, Brück W, Priller J, and Prinz M (2007). Microglia in the adult brain arise from Ly-6ChiCCR2+ monocytes only under defined host conditions. Nat. Neurosci. 10, 1544–1553. 10.1038/nn2015. [PubMed: 18026096]
21. Zhou LJ, Peng J, Xu YN, Zeng WJ, Zhang J, Wei X, Mai CL, Lin ZJ, Liu Y, Murugan M, et al. (2019). Microglia Are Indispensable for Synaptic Plasticity in the Spinal Dorsal Horn and Chronic Pain. Cell Rep. 27, 3844–3859.e6. 10.1016/j.celrep.2019.05.087. [PubMed: 31242418]
22. Peng J, Gu N, Zhou L, B Eyo U, Murugan M, Gan WB, and Wu LJ (2016). Microglia and monocytes synergistically promote the transition from acute to chronic pain after nerve injury. Nat. Commun. 7, 12029. 10.1038/ncomms12029. [PubMed: 27349690]
23. Bedolla AM, McKinsey GL, Ware K, Santander N, Arnold TD, and Luo Y (2024). A comparative evaluation of the strengths and potential caveats of the microglial inducible CreER mouse models. Cell Rep. 43, 113660. 10.1016/j.celrep.2023.113660. [PubMed: 38217856]
24. Faust TE, Feinberg PA, O'Connor C, Kawaguchi R, Chan A, Strasburger H, Frosch M, Boyle MA, Masuda T, Amann L, et al. (2023). A comparative analysis of microglial inducible Cre lines. Cell Rep. 42, 113031. 10.1016/j.celrep.2023.113031. [PubMed: 37635351]
25. Van Hove H, Antunes ARP, De Vlaminck K, Scheyltjens I, Van Ginderachter JA, and Movahedi K (2020). Identifying the variables that drive tamoxifen-independent CreERT2 recombination: Implications for microglial fate mapping and gene deletions. Eur. J. Immunol. 50, 459–463. 10.1002/eji.201948162. [PubMed: 31785096]
26. Prinz M, and Priller J (2010). Tickets to the brain: role of CCR2 andCX3CR1 in myeloid cell entry in the CNS. J. Neuroimmunol. 224, 80–84. 10.1016/j.jneuroim.2010.05.015. [PubMed: 20554025]
27. Guilliams M, Mildner A, and Yona S (2018). Developmental and Functional Heterogeneity of Monocytes. Immunity 49, 595–613. 10.1016/j.immuni.2018.10.005. [PubMed: 30332628]
28. Ginhoux F, Greter M, Leboeuf M, Nandi S, See P, Gokhan S, Mehler MF, Conway SJ, Ng LG, Stanley ER, et al. (2010). Fate mapping analysis reveals that adult microglia derive from primitive macrophages. Science 330, 841–845. 10.1126/science.1194637. [PubMed: 20966214]
29. Jordão MJC, Sankowski R, Brendecke SM, Sagar, Locatelli G., Tai YH., Tay TL., Schramm E., Armbruster S., Hagemeyer N., et al. (2019). Single-cell profiling identifies myeloid cell subsets with distinct fates during neuroinflammation. Science 363, eaat7554. 10.1126/science.aat7554. [PubMed: 30679343]
30. Zhan L, Fan L, Kodama L, Sohn PD, Wong MY, Mousa GA, Zhou Y, Li Y, and Gan L (2020). A MAC2-positive progenitor-like microglial population is resistant to CSF1R inhibition in adult mouse brain. Elife 9, e51796. 10.7554/eLife.51796. [PubMed: 33054973]
31. Saelens W, Cannoodt R, Todorov H, and Saeys Y (2019). A comparison of single-cell trajectory inference methods. Nat. Biotechnol. 37, 547–554. 10.1038/s41587-019-0071-9. [PubMed: 30936559]
32. Cannoodt R, Saelens W, Sichien D, Tavernier S, Janssens S, Guilliams M, Lambrecht B, Preter KD, and Saeys Y (2016). SCORPIUS improves trajectory inference and identifies novel modules in dendritic cell development. Preprint at bioRxiv, 079509. 10.1101/079509.
33. Roth TL, Nayak D, Atanasijevic T, Koretsky AP, Latour LL, and McGavern DB (2014). Transcranial amelioration of inflammation and cell death after brain injury. Nature 505, 223–228. 10.1038/nature12808. [PubMed: 24317693]
34. Doi K, Leelahavanichkul A, Yuen PST, and Star RA (2009). Animal models of sepsis and sepsis-induced kidney injury. J. Clin. Invest. 119, 2868–2878. 10.1172/JCI39421. [PubMed: 19805915]

35. Xaus J, Comalada M, Valledor AF, Lloberas J, López-Soriano F, Argilés JM, Bogdan C, and Celada A (2000). LPS induces apoptosis in macrophages mostly through the autocrine production of TNF-α. Blood 95, 3823–3831. 10.1182/blood.V95.12.3823. [PubMed: 10845916]
36. Varvel NH, Neher JJ, Bosch A, Wang W, Ransohoff RM, Miller RJ, and Dingledine R (2016). Infiltrating monocytes promote brain inflammation and exacerbate neuronal damage after status epilepticus. Proc. Natl. Acad. Sci. USA 113, E5665–E5674. 10.1073/pnas.1604263113. [PubMed: 27601660]
37. Bosco DB, Tian DS, and Wu LJ (2020). Neuroimmune interaction in seizures and epilepsy: focusing on monocyte infiltration. FEBS J. 287, 4822–4837. 10.1111/febs.15428. [PubMed: 32473609]
38. Feng L, Murugan M, Bosco DB, Liu Y, Peng J, Worrell GA, Wang HL, Ta LE, Richardson JR, Shen Y, and Wu LJ (2019). Microglial proliferation and monocyte infiltration contribute to microgliosis following status epilepticus. Glia 67, 1434–1448. 10.1002/glia.23616. [PubMed: 31179602]
39. Willemen HLDM, Eijkelkamp N, Garza Carbajal A, Wang H, Mack M, Zijlstra J, Heijnen CJ, and Kavelaars A (2014). Monocytes/Macrophages control resolution of transient inflammatory pain. J. Pain 15, 496–506. 10.1016/j.jpain.2014.01.491. [PubMed: 24793056]
40. Yan P, Kim KW, Xiao Q, Ma X, Czerniewski LR, Liu H, Rawnsley DR, Yan Y, Randolph GJ, Epelman S, et al. (2022). Peripheral monocyte-derived cells counter amyloid plaque pathogenesis in a mouse model of Alzheimer's disease. J. Clin. Invest. 132, e152565. 10.1172/JCI152565. [PubMed: 35511433]
41. Muñoz-Castro C, Mejias-Ortega M, Sanchez-Mejias E, Navarro V, Trujillo-Estrada L, Jimenez S, Garcia-Leon JA, Fernandez-Valenzuela JJ, Sanchez-Mico MV, Romero-Molina C, et al. (2023). Monocyte-derived cells invade brain parenchyma and amyloid plaques in human Alzheimer's disease hippocampus. Acta Neuropathol. Commun. 11, 31. 10.1186/s40478-023-01530-z. [PubMed: 36855152]
42. Thériault P, ElAli A, and Rivest S (2015). The dynamics of monocytes and microglia in Alzheimer's disease. Alzheimer's Res. Ther. 7, 41. 10.1186/s13195-015-0125-2. [PubMed: 25878730]
43. ElAli A, and Jean LeBlanc N (2016). The Role of Monocytes in Ischemic Stroke Pathobiology: New Avenues to Explore. Front. Aging Neurosci. 8, 29. 10.3389/fnagi.2016.00029. [PubMed: 26941641]
44. Wattananit S, Tornero D, Graubardt N, Memanishvili T, Monni E, Tatarishvili J, Miskinyte G, Ge R, Ahlenius H, Lindvall O, et al. (2016). Monocyte-Derived Macrophages Contribute to Spontaneous Long-Term Functional Recovery after Stroke in Mice. J. Neurosci. 36, 4182–4195. 10.1523/JNEUROSCI.4317-15.2016. [PubMed: 27076418]
45. Chen HR, Sun YY, Chen CW, Kuo YM, Kuan IS, Tiger Li ZR, Short-Miller JC, Smucker MR, and Kuan CY (2020). Fate mapping via CCR2-CreER mice reveals monocyte-to-microglia transition in development and neonatal stroke. Sci. Adv. 6, eabb2119. 10.1126/sciadv.abb2119. [PubMed: 32923636]
46. Carmona-Mora P, Ander BP, Jickling GC, Dykstra-Aiello C, Zhan X, Ferino E, Hamade F, Amini H, Hull H, Sharp FR, and Stamova B (2021). Distinct peripheral blood monocyte and neutrophil transcriptional programs following intracerebral hemorrhage and different etiologies of ischemic stroke. J. Cerebr. Blood Flow Metabol. 41, 1398–1416. 10.1177/0271678X20953912.
47. Alam A, Thelin EP, Tajsic T, Khan DZ, Khellaf A, Patani R, and Helmy A (2020). Cellular infiltration in traumatic brain injury. J. Neuroinflammation 17, 328. 10.1186/s12974-020-02005-x. [PubMed: 33143727]
48. Bauler TJ, Starr T, Nagy TA, Sridhar S, Scott D, Winkler CW, Steele-Mortimer O, Detweiler CS, and Peterson KE (2017). Salmonella Meningitis Associated with Monocyte Infiltration in Mice. Am. J. Pathol. 187, 187–199. 10.1016/j.ajpath.2016.09.002. [PubMed: 27955815]
49. Rua R, Lee JY, Silva AB, Swafford IS, Maric D, Johnson KR, and McGavern DB (2019). Infection drives meningeal engraftment by inflammatory monocytes that impairs CNS immunity. Nat. Immunol. 20, 407–419. 10.1038/s41590-019-0344-y. [PubMed: 30886419]

50. Xu Z, Rao Y, Huang Y, Zhou T, Feng R, Xiong S, Yuan TF, Qin S, Lu Y, Zhou X, et al. (2020). Efficient Strategies for Microglia Replacement in the Central Nervous System. Cell Rep. 32, 108041. 10.1016/j.celrep.2020.108041. [PubMed: 32783928]
51. Ling E-A, Kaur C, and Lu J (1998). Origin, nature, and some functional considerations of intraventricular macrophages, with special reference to the epiplexus cells. Microsc. Res. Tech. 41, 43–56. 10.1002/(sici)1097-0029(19980401)41:1<43::Aid-jemt5>3.0.Co;2-v. [PubMed: 9550136]
52. Serbina NV, and Pamer EG (2006). Monocyte emigration from bone marrow during bacterial infection requires signals mediated by chemokine receptor CCR2. Nat. Immunol. 7, 311–317. 10.1038/ni1309. [PubMed: 16462739]
53. Tsou CL, Peters W, Si Y, Slaymaker S, Aslanian AM, Weisberg SP, Mack M, and Charo IF (2007). Critical roles for CCR2 and MCP-3 in monocyte mobilization from bone marrow and recruitment to inflammatory sites. J. Clin. Invest. 117, 902–909. 10.1172/JCI29919. [PubMed: 17364026]
54. Stuart MJ, Singhal G, and Baune BT (2015). Systematic Review of the Neurobiological Relevance of Chemokines to Psychiatric Disorders. Front. Cell. Neurosci. 9, 357. 10.3389/fncel.2015.00357. [PubMed: 26441528]
55. Bardina SV, Michlmayr D, Hoffman KW, Obara CJ, Sum J, Charo IF, Lu W, Pletnev AG, and Lim JK (2015). Differential Roles of Chemokines CCL2 and CCL7 in Monocytosis and Leukocyte Migration during West Nile Virus Infection. J. Immunol. 195, 4306–4318. 10.4049/jimmunol.1500352. [PubMed: 26401006]
56. Tian DS, Peng J, Murugan M, Feng LJ, Liu JL, Eyo UB, Zhou LJ, Mogilevsky R, Wang W, and Wu LJ (2017). Chemokine CCL2-CCR2 Signaling Induces Neuronal Cell Death via STAT3 Activation and IL-1beta Production after Status Epilepticus. J. Neurosci. 37, 7878–7892. 10.1523/JNEUROSCI.0315-17.2017. [PubMed: 28716963]
57. Takacs GP, Kreiger CJ, Luo D, Tian G, Garcia JS, Deleyrolle LP, Mitchell DA, and Harrison JK (2022). Glioma-derived CCL2 and CCL7 mediate migration of immune suppressive CCR2(+)/CX3CR1(+) M-MDSCs into the tumor microenvironment in a redundant manner. Front. Immunol. 13, 993444. 10.3389/fimmu.2022.993444. [PubMed: 36685592]
58. Shi Z, Yu P, Lin WJ, Chen S, Hu X, Chen S, Cheng J, Liu Q, Yang Y, Li S, et al. (2023). Microglia drive transient insult-induced brain injury by chemotactic recruitment of CD8(+) T lymphocytes. Neuron 111, 696–710.e9. 10.1016/j.neuron.2022.12.009. [PubMed: 36603584]
59. Kim RY, Hoffman AS, Itoh N, Ao Y, Spence R, Sofroniew MV, and Voskuhl RR (2014). Astrocyte CCL2 sustains immune cell infiltration in chronic experimental autoimmune encephalomyelitis. J. Neuroimmunol. 274, 53–61. 10.1016/j.jneuroim.2014.06.009. [PubMed: 25005117]
60. Zhou Y, Tang H, Liu J, Dong J, and Xiong H (2011). Chemokine CCL2 modulation of neuronal excitability and synaptic transmission in rat hippocampal slices. J. Neurochem. 116, 406–414. 10.1111/j.1471-4159.2010.07121.x. [PubMed: 21105875]
61. Yao Y, and Tsirka SE (2014). Monocyte chemoattractant protein-1 and the blood-brain barrier. Cell. Mol. Life Sci. 71, 683–697. 10.1007/s00018-013-1459-1. [PubMed: 24051980]
62. Renner NA, Ivey NS, Redmann RK, Lackner AA, and MacLean AG (2011). MCP-3/CCL7 production by astrocytes: implications for SIV neuroinvasion and AIDS encephalitis. J. Neurovirol. 17, 146–152. 10.1007/s13365-010-0017-y. [PubMed: 21279498]
63. Zhang Y, Chen K, Sloan SA, Bennett ML, Scholze AR, O'Keeffe S, Phatnani HP, Guarnieri P, Caneda C, Ruderisch N, et al. (2014). An RNA-sequencing transcriptome and splicing database of glia, neurons, and vascular cells of the cerebral cortex. J. Neurosci. 34, 11929–11947. 10.1523/JNEUROSCI.1860-14.2014. [PubMed: 25186741]
64. Rayasam A, Kijak JA, Kissel L, Choi YH, Kim T, Hsu M, Joshi D, Laaker CJ, Cismaru P, Lindstedt A, et al. (2022). CXCL13 expressed on inflamed cerebral blood vessels recruit IL-21 producing T(FH) cells to damage neurons following stroke. J. Neuroinflammation 19, 125. 10.1186/s12974-022-02490-2. [PubMed: 35624463]
65. Mastorakos P, and McGavern D (2019). The anatomy and immunology of vasculature in the central nervous system. Sci. Immunol. 4, eaav0492. 10.1126/sciimmunol.aav0492. [PubMed: 31300479]
66. Cui J, Xu H, and Lehtinen MK (2021). Macrophages on the margin: choroid plexus immune responses. Trends Neurosci. 44, 864–875. 10.1016/j.tins.2021.07.002. [PubMed: 34312005]

67. Rustenhoven J, Drieu A, Mamuladze T, de Lima KA, Dykstra T, Wall M, Papadopoulos Z, Kanamori M, Salvador AF, Baker W, et al. (2021). Functional characterization of the dural sinuses as a neuroimmune interface. Cell 184, 1000–1016.e27. 10.1016/j.cell.2020.12.040. [PubMed: 33508229]
68. Møllgård K, Beinlich FRM, Kusk P, Miyakoshi LM, Delle C, Pla V, Hauglund NL, Esmail T, Rasmussen MK, Gomolka RS, et al. (2023). A mesothelium divides the subarachnoid space into functional compartments. Science 379, 84–88. 10.1126/science.adc8810. [PubMed: 36603070]
69. Sjölinder M, Altenbacher G, Hagner M, Sun W, Schedin-Weiss S, and Sjölinder H (2012). Meningococcal outer membrane protein NhhA triggers apoptosis in macrophages. PLoS One 7, e29586. 10.1371/journal.pone.0029586. [PubMed: 22238624]
70. Brouwer MC, Tunkel AR, and van de Beek D (2010). Epidemiology, diagnosis, and antimicrobial treatment of acute bacterial meningitis. Clin. Microbiol. Rev. 23, 467–492. 10.1128/CMR.00070-09. [PubMed: 20610819]
71. Verheul AF, Snippe H, and Poolman JT (1993). Meningococcal lipopolysaccharides: virulence factor and potential vaccine component. Microbiol. Rev. 57, 34–49. 10.1128/mr.57.1.34-49.1993. [PubMed: 8464406]
72. Lu YC, Yeh WC, and Ohashi PS (2008). LPS/TLR4 signal transduction pathway. Cytokine 42, 145–151. 10.1016/j.cyto.2008.01.006. [PubMed: 18304834]
73. De Vlaminck K, Van Hove H, Kancheva D, Scheyltjens I, Pombo Antunes AR, Bastos J, Vara-Perez M, Ali L, Mampay M, Deneyer L, et al. (2022). Differential plasticity and fate of brain-resident and recruited macrophages during the onset and resolution of neuroinflammation. Immunity 55, 2085–2102.e9. 10.1016/j.immuni.2022.09.005. [PubMed: 36228615]
74. Hao Y, Hao S, Andersen-Nissen E, Mauck WM 3rd, Zheng S, Butler A, Lee MJ, Wilk AJ, Darby C, Zager M, et al. (2021). Integrated analysis of multimodal single-cell data. Cell 184, 3573–3587.e29. 10.1016/j.cell.2021.04.048. [PubMed: 34062119]
75. Schneider CA, Rasband WS, and Eliceiri KW (2012). NIH Image to ImageJ: 25 years of image analysis. Nat. Methods 9, 671–675. 10.1038/nmeth.2089. [PubMed: 22930834]
76. Scheyltjens I, Van Hove H, De Vlaminck K, Kancheva D, Bastos J, Vara-Pérez M, Pombo Antunes AR, Martens L, Scott CL, Van Ginderachter JA, et al. (2022). Single-cell RNA and protein profiling of immune cells from the mouse brain and its border tissues. Nat. Protoc. 17, 2354–2388. 10.1038/s41596-022-00716-4. [PubMed: 35931780]
77. Liu YU, Ying Y, Li Y, Eyo UB, Chen T, Zheng J, Umpierre AD, Zhu J, Bosco DB, Dong H, and Wu LJ (2019). Neuronal network activity controls microglial process surveillance in awake mice via norepinephrine signaling. Nat. Neurosci. 22, 1771–1781. 10.1038/s41593-019-0511-3. [PubMed: 31636449]
78. Eyo UB, Haruwaka K, Mo M, Campos-Salazar AB, Wang L, Speros XS 4th, Sabu S, Xu P, and Wu LJ (2021). Microglia provide structural resolution to injured dendrites after severe seizures. Cell Rep. 35, 109080. 10.1016/j.celrep.2021.109080. [PubMed: 33951432]
79. Zheng J, Wang L, Zhao S, Zhang W, Chang Y, Bosco DB, Huang T, Dheer A, Gao S, Xu S, et al. (2023). TREM2 mediates MHCII-associated CD4+ T cell response against gliomas. Neuro Oncol. noad214. 10.1093/neuonc/noad214.
80. Zhao S, Zheng J, Wang L, Umpierre AD, Parusel S, Xie M, Dheer A, Ayasoufi K, Johnson AJ, Richardson JR, and Wu LJ (2023). Chemogenetic manipulation of CX3CR1(+) cells transiently induces hypolocomotion independent of microglia. Mol. Psychiatr. 28, 2857–2871. 10.1038/s41380-023-02128-6.

Highlights

- Border-associated macrophages (BAMs) partially self-repopulate after acute depletion in mice
- $CCR2^{+}$ monocytes engraft brain border and transform into long-lived BAM-like cells
- The BAM-like cells replenish the BAMs under diseased conditions with an initial loss of BAMs
- Microglia do not contribute to the BAM repopulation

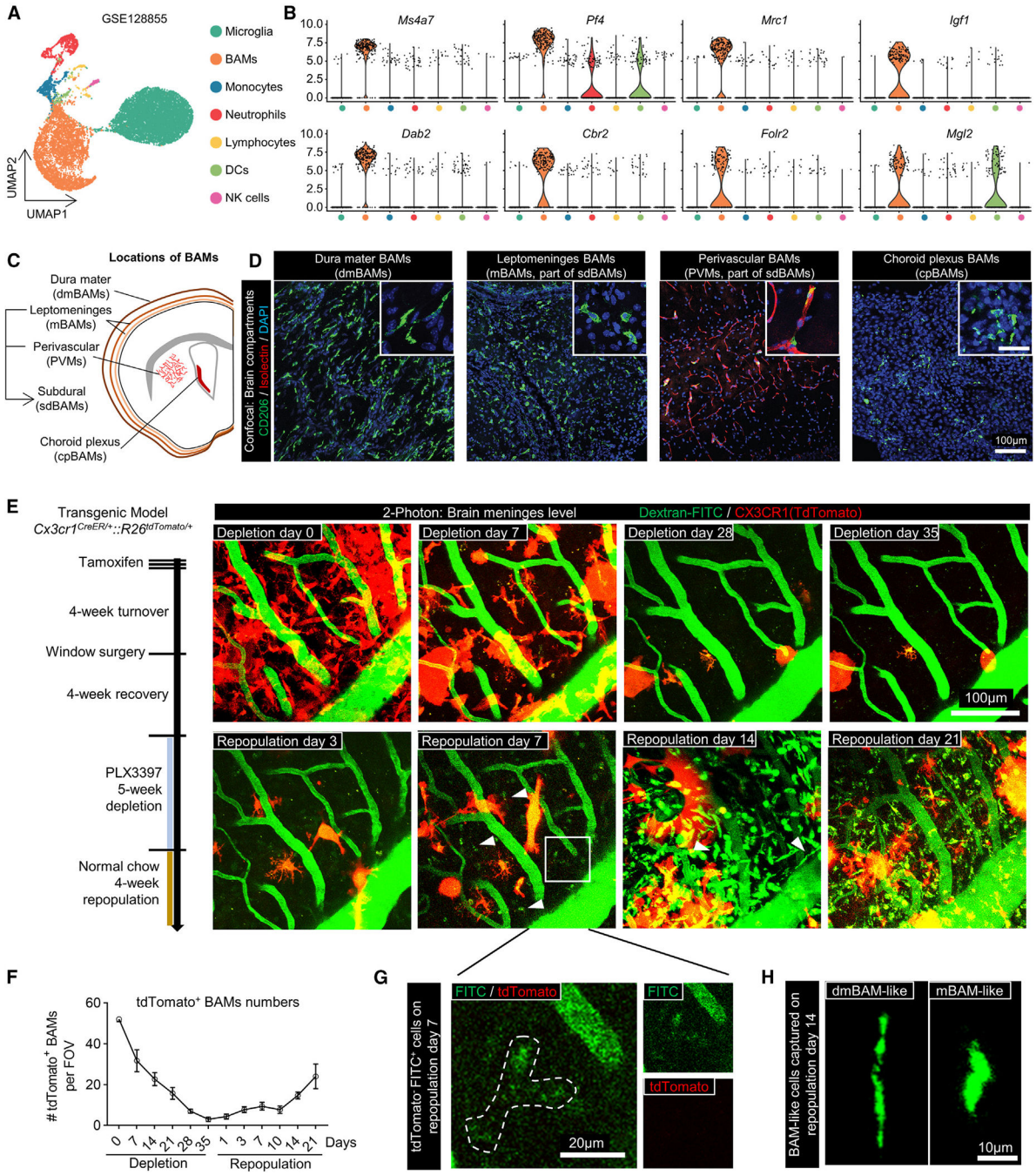

Figure 1. BAMs can partially self-repopulate after depletion.

(A) UMAP plot of immune cell populations collected from the brain and its border in dataset GEO: GSE128855.

(B) Violin plot of the selected top 8 marker genes for BAMs.

(C) Illustration of the brain border compartments and associated BAMs.

(D) Immunostaining of CD206^{+} BAMs from different CNS border compartments. Scale bar, 100 mm and 40 μm (inset).

(E) Two-photon chronic imaging of tdTomato$^+$ BAMs in the meninges and dextran-FITC labeled blood vessels throughout the depletion and repopulation period. White arrowheads show the tdTomato$^-$ FITC$^+$ cells resembling BAMs during repopulation, indicating different origins of the repopulated BAMs. Scale bar, 100 μm.

(F) Quantification of tdTomato$^+$ BAM numbers per 300 × 300 mm^2 field of view throughout the depletion and repopulation (n = 3 mice). Data are presented as mean ± SEM.

(G) Magnified image from (E), showing the tdTomato$^-$ FITC$^+$ cells observed at repopulation day 7 (rectangle in E). Scale bar, 20 μm.

(H) Representative tdTomato$^-$ FITC$^+$ cells resembling dmBAMs and mBAMs at repopulation day 14 (white arrowhead in E). Scale bar, 10 μm.

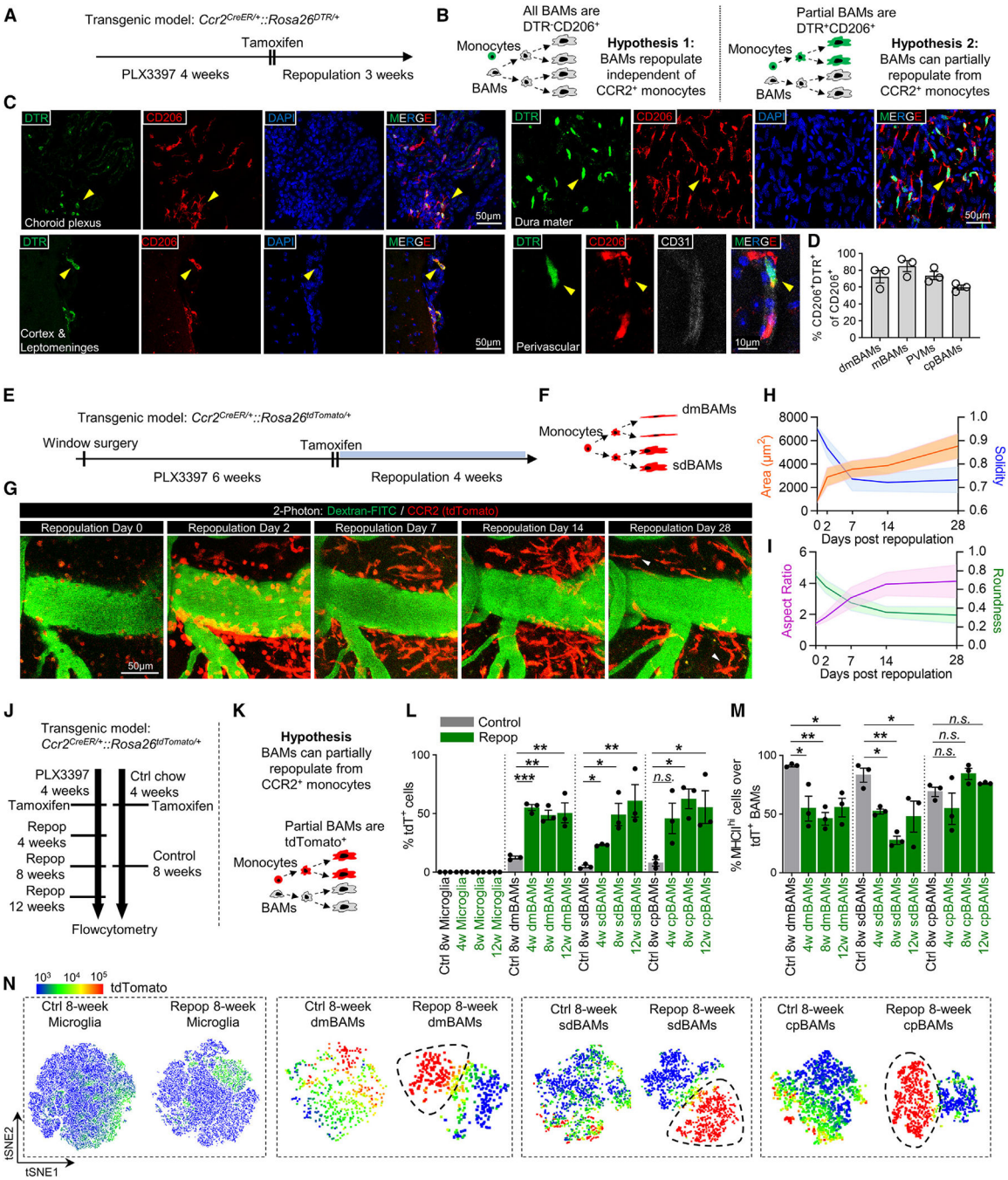

Figure 2. CCR2^{+} monocytes can replenish the depleted BAMs.

(A, B, E, F, J, and K) Illustration of the experiment design, timeline, and hypothesis.

(C) Immunostaining of whole-mount dura mater and choroid plexus and coronal brain slides with leptomeninges attached from *CCR2$^{CreER/+}$::Rosa26$^{DTR/+}$* mice at repopulation week 3. Scale bars, 50 μm and 10 μm as indicated.

(D) Quantification of DTR^{+}CD206^{+} BAMs in different border compartments after repopulation. Data are presented as mean ± SEM (n = 3 mice).

(G–I) Two-photon chronic imaging of the infiltration and transformation of $CCR2^+$ monocytes into BAM-like cells during repopulation. Arrowheads indicate dmBAM-like and mBAMs-like cells at repopulation day 28. Quantification of $CCR2^+$ cell shapes at repopulation days 0, 2, 7, 14, and 28 are presented as mean ±95% confidence interval ($n = 3$ mice).

(L) Percentage of $tdTomato^+$ cells in microglia and BAM subtypes in control and at different repopulation time points. Data are presented as mean ± SEM ($n = 3$ mice). $*p < 0.05$, $**p < 0.01$, $***p < 0.001$, one-way ANOVA with Tukey's multiple-comparisons test.

(M) Percentage of MHC class II^{hi} cells in $tdTomato^+$ BAM subtypes in control and at different repopulation time points. Data are presented as mean ± SEM ($n = 3$ mice). $*p < 0.05$, $**p < 0.01$, one-way ANOVA with Tukey's multiple-comparisons test.

(N) tSNE heatmap of tdTomato expression in microglia and BAM subtypes from both control and repopulated conditions. Dashed circles indicate the $tdTomato^+$ repopulated BAMs.

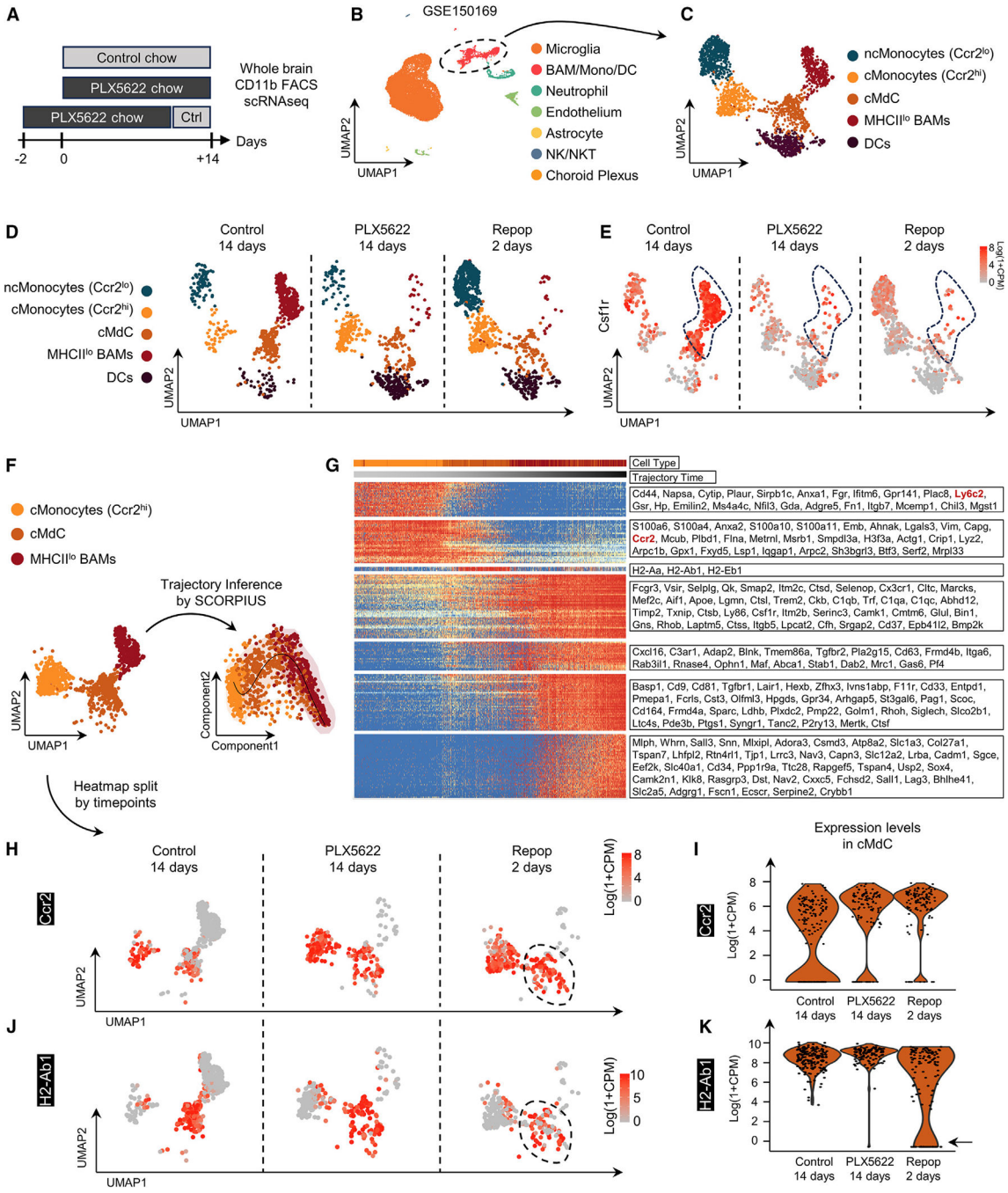

Figure 3. scRNA-seq reveals the close relationship of CCR2^{+} monocytes with the BAMs.

(A) Illustration of the experiment design and group information.

(B) UMAP plot of all cells collected in the dataset GEO: GSE150169.

(C) UMAP plot of the BAMs/monocytes/monocytes-derived cells/DCs from (B).

(D) UMAP plot of the BAMs/monocytes/monocytes-derived cells/DCs split by time points, showing the loss of BAMs induced by PLX5622.

(E) Heatmap of the *Csf1r* gene expression split by time points. Dashed lines indicate the loss of cells with high *Csf1r* expression.

(F) UMAP of classical monocytes (cMonocytes), classical monocyte-derived cells (cMdCs), and the MHC class II^{lo} BAM subset from (C). These three populations were further analyzed by SCORPIUS trajectory inference, where they were linearly aligned along SCORPIUS component 1.

(G) The top 250 genes corresponding to the transition from monocytes to BAMs that were clustered by different gene expression trends, showing a gradientdecrease of monocyte markers and increase of BAM markers.

(H and J) Heatmaps of cMonocytes, cMdC, MHC class II^{lo} BAMs from (F), split by time points, showing the expression of the *Ccr2* and *H2-Ab1* genes. Dashed circles indicate the cMdC population.

(I and K) Violin plots of cMonocytes, cMdCs, and MHC class II^{lo} BAMs corresponding to (H) and (J), showing the distribution of *Ccr2* and *H2-Ab1* expression in cMdCs at different time points. Arrows indicate the increased portion of the CCR2^{hi}MHC class II$^{lo/neg}$ cells in the cMdC cluster at repopulation day 2.

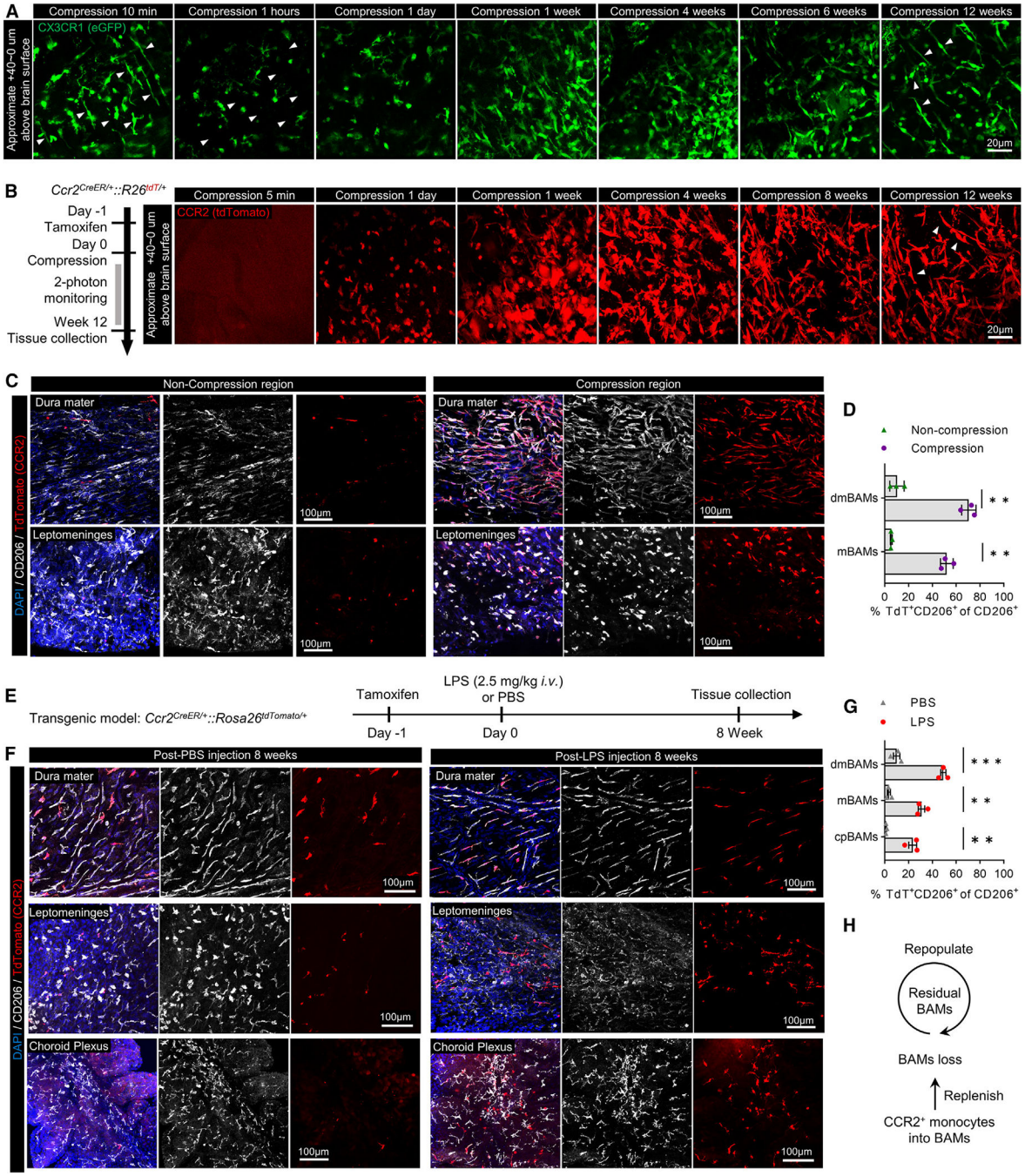

Figure 4. Long-term engraftment and transformation of CCR2^{+} monocytes into BAMs in the diseased brain.

(A) Two-photon chronic imaging showing the acute loss of dmBAMs and mBAMs after mild cortical compression and the chronic replenishment of these cells inthe *Cx3cr1*$^{Gfp/+}$ mice. Arrowheads indicate dmBAMs and mBAMs. Scale bar, 20 μm.

(B) Two-photon chronic imaging showing the infiltration and transformation of CCR2^{+} monocytes into dmBAM-like and mBAM-like cells in the meninges 12 weeks after mild cortical compression in *Ccr2*$^{CreER/+}$*::R26*$^{tdTomato/+}$ mice. Scale bars, 20 μm.

(C and D) Immunostaining of the dura mater and leptomeninges and quantifications of tdTomato^{+}CD206^{+} BAMs in the compression and non-compression regions at 12 weeks post injury. Data are presented as mean ± SEM (n = 3 mice). $^{**}p < 0.01$, paired t test.
(E) Illustration of the study plan and timeline.
(F and G) Immunostaining and quantifications of tdTomato^{+}CD206^{+} BAMs in the dura mater and leptomeninges at 8 weeks post LPS or PBS injection. Data are presented as mean ± SEM (n = 3 mice). $^{**}p < 0.01$, $^{***}p < 0.001$, unpaired t test. Scale bars, 100 μm.
(H) Illustration of our conclusion that CCR2^{+} monocytes could replenish the lost BAMs in addition to BAM self-proliferation.

KEY RESOURCES TABLE

REAGENT or RESOURCE	SOURCE	IDENTIFIER
Antibodies		
Rat anti Mouse CD206	BIO-RAD	MCA2235; RRID: AB_324622
Goat anti Mouse CD206	R&D	AF2535; RRID: AB_2063012
Goat anti Human DTR (HB-EGF)	R&D	AF-259-NA; RRID: AB_354429
Rat anti Mouse CD31	BD BIOSCIENCE	550274; RRID: AB_393571
Goat anti Mouse CD31	NOVUS BIOLOGICALS	AF3628; RRID: AB_2161028
Rabbit anti Mouse IBA1	Abcam	AB178847; RRID: AB_2832244
Rabbit anti Mouse PDGFRa	Abcam	AB203491; RRID: AB_2892065
Rat anti Mouse MHCII	Invitrogen	14–5321-82; RRID: AB_467561
Goat anti Rat Alexa Fluor™ 555	Invitrogen	A21434; RRID: AB_2535855
Goat anti Rat Alexa Fluor™ 647	Invitrogen	A21247; RRID: AB_141778
Donkey anti Goat Alexa Fluor™ 488	Invitrogen	A11055; RRID: AB_2534102
Donkey anti Goat Alexa Fluor™ 594	Invitrogen	A11058; RRID: AB_2534105
Donkey anti Goat Alexa Fluor™ 647	Invitrogen	A21447; RRID: AB_2535864
APC/Fire810 anti-NK1.1	BioLegend	156519; RRID: AB_2894654
BB700 anti-MHC II	BD Biosciences	746197; RRID: AB_2743544
APC anti-Ly6G	BD Biosciences	560599; RRID: AB_1727560
PE-CF594 anti-CD45	BD Biosciences	562420; RRID: AB_11154401
PE-Cy5 anti-CD11b	Tonbo Biosciences	55–0112; RRID: AB_2621818
PE-Cy7 anti-TCRβ	Biolegend	109221; RRID: AB_893625
Spark NIR 685 anti-B220	BioLegend	103267; RRID: AB_2819759
Chemicals, peptides, and recombinant proteins		
Lycopersicon Esculentum (Tomato) Lectin (LEL, TL), DyLight™ 594	Vector Lab	DL-1177–1
DAPI Fluoromount-G	SouthernBiotech	0100–20
Dextran, Fluorescein, 70,000 MW, Anionic	Invitrogen	D1823
Dextran, Fluorescein, 10,000 MW, Anionic	Invitrogen	D1821
PLX-3397 (Pexidartinib)	Chemgood	C-1271
Lipopolysaccharides	Sigma-Aldrich	L2880
Ghost Dye™ Red 780	Tonbo Biosciences	13–0865
Tamoxifen	Sigma-Aldrich	T5648
Deposited data		
Single-cell RNAseq dataset	Van Hove et al.[9]	GEO: GSE128855, https://www.ncbi.nlm.nih.gov/geo/query/acc.cgi?acc=GSE128855
Single-cell RNAseq dataset	Jordão et al.[29]	GEO: GSE118948, https://www.ncbi.nlm.nih.gov/geo/query/acc.cgi?acc=GSE118948

REAGENT or RESOURCE	SOURCE	IDENTIFIER
Single-cell RNAseq dataset	Zhan et al.[30]	GEO: GSE150169, https://www.ncbi.nlm.nih.gov/geo/query/acc.cgi?acc=GSE150169
Experimental models: Organisms/strains		
Mouse: *B6.129P2(C)-Cx3cr1$^{tm2.1(cre/ERT2)Jung}$/J*	The Jackson Laboratory	JAX:020940
Mouse: *B6.Cg-Gt(ROSA)26Sor$^{tm14(CAG-tdTomato)Hze}$/J*	The Jackson Laboratory	JAX:007914
Mouse: *C57BL/6-Ccr2$^{em1(icre/ERT2)Peng}$/J*	The Jackson Laboratory	JAX:035229
Mouse: *C57BL/6-Gt(ROSA)26Sor$^{tm1(HBEGF)Awai}$/J*	The Jackson Laboratory	JAX:007900
Mouse: *CCR2^{CreER}*	From Dr. Chia-Yi Kuan, University of Virginia	N/A
Mouse: *Tmem119$^{em1(cre/ERT2)Gfng}$/J*	The Jackson Laboratory	JAX:031820
Software and algorithms		
Seurat	Hao et al.[74]	https://github.com/satijalab/seurat
SCORPIUS	Cannoodt et al.[32]	https://github.com/rcannood/SCORPIUS
ImageJ	Schneider et al.[75]	https://fiji.sc/
GraphPad Prism	Dotmatics	https://www.graphpad.com/
R	R Core Team	https://cran.r-project.org/
RStudio/POSIT	RStudio Team	https://posit.co/downloads/
SpectroFlo	Cytek Biosciences	https://cytekbio.com/pages/spectro-flo
FlowJo	BD Life Sciences	https://www.flowjo.com/solutions/flowjo/downloads
BioRender	BioRender	https://www.biorender.com/
Codes for single-cell RNAseq analysis	This study	https://zenodo.org/doi/10.5281/zenodo.10836090
Other		
Confocal microscope	Zeiss	LSM980
Dental drill	Osada	EXLM40
Hydrogen peroxide	McKesson	#23-D0012
4-mm glass coverslip	Warner Instruments	64–0724
5-mm glass coverslip	Warner Instruments	64–0700
Dental glue - Tetric EvoFlow	Ivoclar	595954WW
Dental glue - iBond Total Etch glue	Kulzer	https://www.kulzer.com/en/en/products/ibond-total-etch.html
Four-point head plate	Neurotar	Model 4, https://www.neurotar.com/support/guide-to-head-plates/
Multiphoton microscope	Scientifica	https://www.scientifica.uk.com/products/scientifica-hyperscope
Mai-Tai DeepSee laser	Mai Tai	https://www.spectra-physics.com/en/f/mai-tai-deepsee-ultrafast-laser
Spectral flow cytometer	Cytek Biosciences	Cytek Aurora